PDF Preprint

Han, T., M.A. Wulder, J.C. White, N.C. Coops, M.F. Alvarez, and C. Butson, 2007; An efficient protocol to process Landsat images for change detection with Tasselled Cap Transformation, IEEE Geoscience and Remote Sensing Letters, 4(1):147-151.

There may be minor editorial differences between this version and the paper published in IEEE Geoscience and Remote Sensing Letters.

An efficient protocol to process Landsat images for change detection with Tasselled Cap Transformation

T. Han, M.A. Wulder*, J.C. White, N.C. Coops, M.F. Alvarez, and C. Butson

T. Han is with Canadian Forest Service (Pacific Forestry Centre), Natural Resources Canada, Victoria, British Columbia. (email: than@nrcan.gc.ca).

M.A. Wulder is with Canadian Forest Service (Pacific Forestry Centre), Natural Resources Canada, Victoria, British Columbia.
*(Corresponding author. Phone: (250) 363-6090; fax: (250) 363-0775; email: mwulder@nrcan.gc.ca).

J.C. White is with Canadian Forest Service (Pacific Forestry Centre), Natural Resources Canada, Victoria, British Columbia. (email: joanne.white@nrcan.gc.ca).

N.C. Coops is with the Department of Forest Resource Management, University of British Columbia, Vancouver, British Columbia (email: nicholas.coops@ubc.ca).

M.F. Alvarez is with Department of Geodesy, Cartography and Photogrammetry Engineering, Universidad de Leon, E.S.T., Ponferrada, Leon, Spain (email: flor.alvarez@unileon.es).

C. Butson is with Canadian Forest Service (Pacific Forestry Centre), Natural Resources Canada, Victoria, British Columbia. (email: chris.butson@nrcan.gc.ca).

ABSTRACT

Change detection approaches, such as computing change in spectral indices through time, are a mature and established science, which is increasingly being applied in operational remote sensing programs. The quality and consistency of the changes detected using these approaches are linked however to the processing of the imagery which is required to address issues related to image radiometry, normalization, and computation of the spectral indices. These processing steps are typically undertaken independently providing opportunities for computation errors, increasing disk storage needs, and consuming processing time. In this communication we present an approach for combining these processing steps to facilitate a more streamlined and computationally efficient approach to change detection using Landsat 5 and 7. The individual elements of the algorithm (raw Landsat-5 or -7, to calibrated Landsat-7, to top-of-atmosphere reflectance, to Tasselled Cap components) are described, followed by a description and illustration of the protocol to algebraically combine the elements. Rather than producing intermediate outputs, the sequentially integrated data processing protocol operates in memory and produces only the desired outputs. The proposed approach mitigates opportunities for inappropriate scaling between processing steps, the consistency of which is especially important for threshold based change detection procedures. In addition, savings in both processing time and disk storage are afforded through the combination of processing steps, with processing of the time-1 images reduced from 3 to 2 stages and 5 to 2 stages for the time-2 images, resulting in savings of 50% and 69% in computing times and disk space requirements respectively.

Index Terms: Change detection, Landsat data correction, Tasselled Cap Transformation, Mountain Pine Beetle red attack, Enhanced Wetness Difference Index

I. INTRODUCTION

At the broad scale, Landsat data, in particular when processed using change detection approaches, has successfully been applied in an increasing number of studies to detect and map forest damage attributable to the mountain pine beetle [1]. A number of change detection techniques have been used to assess variations in forest condition [2][3][4]. Prominent among the approaches identified as having operational potential is the use of the Tasselled Cap Transformation (TCT) [5] which has been shown to capture forest changes due to harvest [6][7], fire [8][9], and insects [1][10][11][12]. Fundamentally, TCT is a guided and scaled transformation, which converts Landsat bands into channels of known characteristics: soil brightness, vegetation greenness, and soil/vegetation wetness. Although TCT was initially proposed for agricultural applications, it has been found to be sensitive to structural characteristics of forest environments [13]. One key advantage of the TCT method over other statistical methods such as principal component analysis (PCA) is that TCT is independent of the individual scenes, while PCA is dependent on the scene being processed [4]. Changes in these TCT components over time can therefore be related to changes in the vegetation characteristics. In particular, changes in the TCT wetness components have been identified as a reliable indicator of forest change [10]. Using this approach [1] proposed the Enhanced Wetness Difference Index (EWDI) which is calculated as the difference between two wetness indices derived from the TCT of Landsat images acquired over differing dates. As an example, in areas undergoing mountain pine beetle attack, positive EWDI values indicate areas of reduced wetness, and are therefore indicative of disturbed forests. Negative EWDI values represent wetness gain, indicative of areas of re-growth. Areas with close-to-zero EWDI values represent pixels with no observed change.

For the successful application of this technique, both input Landsat images need to be processed using a series of radiometric corrections and normalizations that reduce the spectral variations that may be related to different sensor characteristics, atmospheric conditions, and viewing and illuminating geometries [14]. These processing steps are applied to each pixel of the input images. The sequential execution of these processing steps is time consuming and storage intensive. Moreover, the errors arising from improper between-step scaling may impact the effectiveness of thresholding based change detection techniques. EWDI is such a technique, based on thresholding the difference of TCT wetness indices, to identify forest changes over time. The determination of the optimal threshold value is a critical task. Using inappropriate threshold values undermines the reliability of change detection and produces erroneous change maps.

In this communication, these separate data processing steps are integrated through linear transformations (translation, rotation, and scaling). To demonstrate this simplified approach the technique proposed by [1] is revisited and enhanced with the integrated steps. The following objectives are addressed: 1. to propose an integrated approach for Landsat data radiometric correction and normalization; 2. to indicate the impact of the improper scaling on calculating TCT wetness index values; 3. to demonstrate the usefulness of the proposed approach with respect to mitigating scaling errors and saving computing resources; 4. to serve as a concise source of information for change detection applications with Landsat imagery. This ready and tested approach is intended to help users, especially new users, focus on the results of change analyses, rather than gathering and vetting the appropriate formulas and coefficients from a diverse collection of scientific literature.

II. STUDY AREA AND IMAGERY

Demonstration of the proposed technique is over the Merritt Timber Supply Area (TSA), located in the south-western interior of British Columbia, Canada (Figure 1). Forests in this area are dominated by lodgepole pine, Douglas-fir, and spruce, with 14% of the forest stands identified as 100% lodgepole pine from the current field based forest inventory [12]. Four images acquired on two dates were selected for analysis (Table 1). They were all orthorectified [15]. Since the two images (path 46, rows 25 and 26) were sequentially collected on the same date, mosaicking was undertaken, using ENVI map tools [16], to create a seamless image for each date (August 14, 2002 and September 28, 2004).

<<Figure 1 here>>

<<Table 1 here>>

III. INTEGRATED DATA PROCESSING

As the EWDI is calculated based on the TCT wetness indices derived from two input images [1], any variations between the inputs that are not indicative of wetness changes should be minimized prior to TCT transformation. Sources of such variations include different sensor characteristics, atmospheric conditions, and view and illumination geometries. A series of processing steps is proposed to reduce these possible sources of variation. The processing steps comprise between-sensor DN conversion, top-of-atmosphere (TOA) radiance correction, TOA-reflectance correction, and normalization. The between-sensor DN conversion is used to compensate between-sensor differences in gain, offset, spectral response function, and signal-to-noise ratio when input images were acquired by different sensors. The TOA-radiance and reflectance corrections are employed for atmospheric correction when *in-situ* measurements of atmospheric and climate conditions at the time of image acquisition are unknown and the imagery was acquired under clear-sky conditions. Using the gain and offset derived from dark and bright targets, the normalization is conducted to reduce image discrepancies possibly remaining from differing illumination geometries of the input imagery that were not fully addressed by the TOA-corrections.

<<Figure 2 here>>

The applicability of the proceeding processing steps is dependent on status of the input images. For example, if both input images are collected by the same sensor, the step of between-sensor DN conversion will be dropped. Tailored to the images used in this study where the time-1 input is in orthorectified ETM+ raw DN and the time-2 input is in orthorectified TM raw DN, the data processing, as shown in Figure 2, incorporates three steps for the time-1 input and five steps for the time-2 input. Normally these steps are executed sequentially and repeated for each pixel in the input images. However, the sequential execution consumes both time and disk space, particularly when large images are processed, and may also introduce possible sources of error due to improper scaling between processing steps. An integrated procedure with fewer processing steps is accordingly desired. In this section, a method of integration is proposed, which aggregates the processing steps separately required by the time-1 and -2 input images.

A. Integrated processing for time-1 image

As shown in Figure 2, the three processing steps for the time-1 input image are: TOA-radiance correction, TOA-reflectance correction, and TCT transformation. Ideally these can be integrated into a single step. However, considering that the normalization of the time-2 image requires the TOA-reflectance of the time-1 image, the first two TOA-correction steps are combined instead, leaving the TCT transformation as a separate step. The two TOA-correction steps are combined as follows: Let $\vec{x}=[x_1,...,x_6]^T$ be the column vector representing a pixel of the input image; $\vec{g}^1=[g_1^1,...,g_6^1]^T$ be the column vector representing the gain of radiance correction; $\vec{o}^1=[o_1^1,...,o_6^1]^T$ be the column vector representing the offset of radiance correction; and $\vec{y}^1=[y_1^1,...,y_6^1]^T$ be the column vector representing the TOA-radiance of $\vec{x}$. Then $y_i^1=g_i^1\times x_i+o_i^1$ for $i=1,...,6$. This equation can be expressed equivalently in the following matrix format:

$$\vec{y}^1=G^1\vec{x}+\vec{o}^1=\begin{bmatrix} g_1^1 & 0 & ... & 0 \\ 0 & g_2^1 & ... & 0 \\ ... & ... & ... & ... \\ 0 & 0 & ... & g_6^1 \end{bmatrix}\begin{bmatrix} x_1 \\ x_2 \\ ... \\ x_6 \end{bmatrix}+\begin{bmatrix} o_1^1 \\ o_2^1 \\ ... \\ o_6^1 \end{bmatrix} \quad (1)$$

Note that all the superscripts used in this derivation and those that follow, are labels indicative of data processing levels. The TOA-reflectance correction is conducted similarly as follows. Let $\vec{g}^2=[g_1^2,...,g_6^2]^T$ be the column vector representing the gain of TOA-reflectance correction; $\vec{y}^2=[y_1^2,...,y_6^2]^T$ be the column vector representing TOA-reflectance of $\vec{x}$. Then $y_i^2=g_i^2\times y_i^1$, for $i=1,2,...,6$, which can be represented in the following matrix format:

$$\vec{y}^2 = G^2\vec{y}^1 = \begin{bmatrix} g_1^2 & 0 & \dots & 0 \\ 0 & g_2^2 & \dots & 0 \\ \dots & \dots & \dots & \dots \\ 0 & 0 & \dots & g_6^2 \end{bmatrix} \begin{bmatrix} y_1^1 \\ y_2^1 \\ \dots \\ y_6^1 \end{bmatrix} \quad (2)$$

The above TOA-corrections are combined by substituting $\vec{y}^1$ in (2) with (1), which produces:

$$\vec{y}^2 = G^2\vec{y}^1 = G^2(G^1\vec{x} + \vec{o}^1)$$
$$= \begin{bmatrix} g_1^2 & 0 & \dots & 0 \\ 0 & g_2^2 & \dots & 0 \\ \dots & \dots & \dots & \dots \\ 0 & 0 & \dots & g_6^2 \end{bmatrix} [\begin{bmatrix} g_1^1 & 0 & \dots & 0 \\ 0 & g_2^1 & \dots & 0 \\ \dots & \dots & \dots & \dots \\ 0 & 0 & \dots & g_6^1 \end{bmatrix} \begin{bmatrix} x_1 \\ x_2 \\ \dots \\ x_6 \end{bmatrix} + \begin{bmatrix} o_1^1 \\ o_2^1 \\ \dots \\ o_6^1 \end{bmatrix}] \quad (3)$$

Based on the TOA reflectance ($\vec{y}^2$), TCT wetness index is calculated separately, $wi_1 = \sum_{i=1}^{6} c_i \times y_i^2$, or equivalently:

$$wi_1 = \vec{c}^T\vec{y}^2 = [c_1,\dots,c_6][y_1^2,\dots,y_6^2]^T \quad (4)$$

where wi_1 is the TCT wetness index of the pixel $\vec{x}$ in the time-1 image, and $\vec{c} = [c_1,\dots,c_6]^T$ be the column vector of the TCT wetness coefficients.

B. Integrated processing for time-2 image

For processing the time-2 image, there are five steps: (i) conversion of TM to ETM+, (ii) TOA-radiance correction, (iii) TOA-reflectance correction, (iv) normalization, and (v) TCT wetness calculation. The first three steps are merged into one step, and the last two steps are combined into another. Let $\vec{x} = [x_1,\dots,x_6]^T$ be the column vector representing a pixel in the time-2 image (Landsat TM); $\vec{g}^1 = [g_1^1,\dots,g_6^1]^T$ be the column vector representing the conversion gain from TM to ETM+; $\vec{o}^1 = [o_1^1,\dots,o_6^1]^T$ be the column vector representing the conversion offset; $\vec{y}^1 = [y_1^1,\dots,y_6^1]^T$ be the column vector representing the converted result of $\vec{x}$. Then $y_i^1 = g_i^1 \times x_i + o_i^1$ for $i = 1,2,\dots,6$. This equation can be expressed equivalently as the following matrix format:

$$\vec{y}^1 = G^1\vec{x} + \vec{o}^1 = \begin{bmatrix} g_1^1 & 0 & \dots & 0 \\ 0 & g_2^1 & \dots & 0 \\ \dots & \dots & \dots & \dots \\ 0 & 0 & \dots & g_6^1 \end{bmatrix} \begin{bmatrix} x_1 \\ x_2 \\ \dots \\ x_6 \end{bmatrix} + \begin{bmatrix} o_1^1 \\ o_2^1 \\ \dots \\ o_6^1 \end{bmatrix} \quad (5)$$

The TOA-corrections are conducted in the same way as in (1) and (2), and combined with (5). The integrated correction is:

$$\vec{y}^3 = G^3(G^2(G^1\vec{x} + \vec{o}^1) + \vec{o}^2) \quad (6)$$

where $\vec{o}^2$: TOA-radiance correction offset vector;

G^2 : TOA-radiance correction gain matrix;

G^3 : TOA-reflectance correction gain matrix;

$\vec{y}^3$: corrected result of pixel $\vec{x}$.

The last two steps for correcting the time-2 image, normalization and TCT wetness calculation, are combined on the basis of the TOA-reflectance $\vec{y}^3$, which is:

$$wi_2 = \vec{c}^T(G^4\vec{y}^3 + \vec{o}^4) \quad (7)$$

where $\vec{o}^4$: normalization correction offset vector;

G^4 : normalization correction gain matrix;

$\vec{c}$: TCT coefficient vector;

wi_2 : TCT wetness index of pixel $\vec{x}$.

Now the correction steps for the time-1 image have been reduced from three to two (as given in (3) and (4)), and for the time-2 image the correction steps have been reduced from five to two (as given in (6) and (7)). All the coefficients involved can be found in [17 – 22].

C. Calculation of Enhanced Wetness Difference Index (EWDI)

The final step is the calculation of EWDI:

$$EWDI = wi_1 - wi_2 \quad (8)$$

where wi_1 and wi_2 are the TCT wetness indices derived from the time-1 and -2 images, respectively. They are calculated with (4) and (7). As a result, large positive EWDI values indicate wetness loss, while small EWDI values indicate a lack of change in wetness. Large negative EWDI values represent wetness gain. Areas with large positive values in the EWDI image are likely to be the mountain pine beetle red attack areas. However, mountain pine beetle red attack is not the only disturbance that causes wetness loss. Other disturbances, chiefly harvesting and fire, also result in wetness loss. It is critical to separate these disturbances through masking. A pine mask is applied to constrain analyses to applicable areas; followed by a thresholding approach to focus upon wetness difference values that can be attributed to mountain pine beetle red attack (details presented in [1][12]).

V. RESULTS AND DISCUSSION

The focus of this communication is on the integrated processing protocol, with an application example dataset used to demonstrate a context and to illustrate the viability of the approach. Results of the application, such as accuracy assessment, can be found in [1][12]. It should be pointed out that the protocol is fully functional, as per the step-by-step implementation of the data processing tasks outlined in Figure 2, providing the intermediate results out of each step are stored with adequate precision (2-byte integer or 4-byte floating point). Applications based on Landsat data, however, tend to save the intermediate results in byte. This tendency may be because Landsat data are provided in byte or the storage space is limited. No matter which one is relevant, saving the intermediate results in byte involves data scaling. Improper scaling may result in erroneous outcome, which affect subsequent data processing.

<<Table 2 here>>

To demonstrate the impact of such scaling on calculating TCT wetness indices, the standard flow of the data processing shown in Figure 2 was implemented. The intermediate results out of each step were scaled to fit the range of [0, 255] and saved on a hard disk. Meanwhile the integrated approach proposed in the previous section was implemented as well. Contrary to the standard approach, the integrated approach kept the reduced intermediate results in floating point without scaling. Table 2 shows the migration of an arbitrarily selected forest pixel spectrum (from the time-2 image) in data flow, where the values in bold italic were from the integrated approach. The TCT wetness index calculated using the standard approach was -18, while the corresponding value calculated using the integrated approach was -20.

<<Figure 3 here>>

To complement the above experiment based on a single pixel, the impact of scaling was investigated by using the entire time-2 dataset. Histograms were produced of the wetness index images derived from both standard and integrated approaches. As shown in Figure 3, the scaling caused changes in the density distribution of wetness values are clear. It can be anticipated that such changes will affect subsequent analysis dependent on TCT wetness values. The altered, possibly inconsistent, wetness index values have implications to the change detection methods, especially those based on thresholding.

<<Table 3 here>>

The other advantage of the integrated approach lies on saving computing time and storage space. In Table 3 the storage and computation time implications of the standard versus integrated implementation are provided. Disk space and computing time are based upon a subset taken from the time-2 input (Landsat TM) resulting in an image size of 3655 pixels and 5495 lines, with six 8-bit channels. This benchmark test is conducted on a SUN workstation (SUN4U with 4GB memory). The benchmark indicates that when compared to the standard approach, the integrated approach saves 50% and 69% in computing time and disk space, respectively. These savings, seemingly insignificant for a few datasets of small sizes, may have tremendous impact for land cover mapping or change detection applications using many images covering large areas. Large, national or continental, areas are increasingly mapped and monitored for change over time [23]. Hundreds of images must be processed to meet the monitoring and mapping objectives of these large area initiatives. Any savings, in time or disk space, increase the operational feasibility of large area mapping and monitoring programs. The consistency of information generated enables increased opportunities for automated analyses and buttresses user confidence in data for analysis and results subsequently arrived at.

VI. CONCLUSION

In this study, we reviewed the steps required to process multi-date Landsat images for change detection purposes. The issues associated with the sequential application of these steps were discussed and an integrated processing approach was proposed, which reduced the 3-step processing of the time-1 image to 2, and the 5-step processing of the time-2 image to 2. Benchmark testing indicates that compared to the standard data flow, the combined data flow can save 50% and 69% in computing time and disk space, respectively. Moreover, the integrated approach requires fewer data scaling steps with resultant improvements in numerical consistency, an important factor when relative differences between image dates are being assessed. The integrated approach is applied to process two-date Landsat-5 TM and -7 ETM+ images for the mapping of mountain pine beetle infestations at a site in south central British Columbia, Canada.

Though the integrated approach is demonstrated with respect to Landsat datasets, it can be applied to other remotely sensed datasets by substituting the coefficients in Equation (3), (4), (6), and (7) with the corresponding values appropriate for other datasets under consideration. There is a wide range of applications for change detection [3][24], utilizing different spectral indices [7][25][26][27]. The availably of an integrated processing protocol to mitigate possible data-scaling errors, to reduce disk storage needs, and to decrease processing times is applicable to a range of user communities and applications areas.

Acknowledgements: This project is funded by the Government of Canada through the Mountain Pine Beetle Initiative, a six-year, $40 million program administered by Natural Resources Canada, Canadian Forest Service. Additional information on the Mountain Pine Beetle Initiative may be found at: http://mpb.cfs.nrcan.gc.ca/.

REFERENCES

[1] Skakun, R.S., M.A. Wulder and S.E. Franklin, 2003. Sensitivity of the thematic mapper enhanced wetness difference index to detect mountain pine beetle red-attack damage. *Remote Sensing of Environment*, 86:433-443.

[2] Gong, P. and B. Xu, 2003. Remote sensing of forests over time: change types, methods, and opportunities, Remote Sensing of Forest Environments: Concepts and Case Studies, Edited by M.A. Wulder and S.E. Franklin, Kluwer Academic Publishers, Massachusetts. pp. 301-333.

[3] Coppin, P., I. Jonckheere, K. Nackaerts, and B. Muys, 2004. Digital change detection methods in ecosystem monitoring: a review. *International Journal of Remote Sensing*, *25*: 1565-1596.

[4] Lu, D., Mausel, P., Bronzdizio, E., and E. Moran, 2004. Change detection techniques. *International Journal of Remote Sensing, 25*: 2365-2407.

[5] Crist, E. P., and R. C. Cicone, 1984, A physically-based transformation of Thematic Mapper data – the TM Tasselled Cap, *IEEE Trans. On Geoscience and Remote Sensing*, GE-22:256-263.

[6] Cohen, W.B., M. Fiorella, J. Gray, E. Helmer, and K. Anderson, 1998. An efficient and accurate method for mapping forest clearcuts in the Pacific Northwest using Landsat imagery. *Photogrammetric Engineering and Remote Sensing, 64*: 293-300.

[7] Jin, S. and S. Sader, 2005. Comparison of time series Tasselled cap wetness and the normalized difference moisture index in detecting forest disturbances. *Remote Sensing of Environment, 94*: 364-372.

[8] Cohen, W.B., T.A. Spies, R.J. Alig, D.R. Oetter, T.K. Maiersperger, and M. Fiorella, 2002. Characterizing 23 years (1972-95) of stand replacement disturbance in Western Oregon forest with Landsat imagery. *Ecosystems*, 122-137.

[9] Healey, S.P., W. B. Cohen, Y. Zhiqiang, and O.N. Krankina, 2005. Comparison of Tasselled cap-based Landsat data structures for use in forest disturbance detection. *Remote Sensing of Environment, 97*: 301-310.

[10] Collins, J.B. and C.E. Woodcock, 1996. An assessment of several linear change detection techniques for mapping forest mortality using multitemporal Landsat TM data. *Remote Sensing of Environment, 56*: 66-77.

[11] Price, K.P. and M.E. Jakubauskas, 1998. Spectral retrogression and insect damage in lodgepole pine successional forests. *International Journal of Remote Sensing, 19*: 1627-1632.

[12] Wulder, M.A., J.C. White, N.C. Coops, T. Han, M.F. Alvarez, C.R. Butson and X Yuan, 2006. A Procedure For Mapping and Monitoring Mountain Pine Beetle Red Attack Forest Damage Using Landsat Imagery. Natural Resources Canada, Canadian Forest Service, Pacific Forestry Centre Information Report BC-X-404, Victoria, British Columbia

[13] Cohen, W. B., T. A. Spies, and M. Fiorella, 1995. Estimating the age and structure of forests in a multi-ownership landscape of Western Oregon, U.S.A. *International Journal of Remote Sensing*, 16: 721-746.

[14] Peddle, D.R., P.M. Teillet and M.A. Wulder, 2003. Radiometric Image Processing. Invited Book Chapter in "Remote Sensing of Forest Environments: Concepts and Case Studies". Kluwer Academic Press, London/Dordrecht/Boston (Norwell, Massachusetts, USA). pp.181-208.

[15] BC Ministry of Forests and Range, Forest Analysis and Inventory Branch Landsat 5 Orthorectification and Processing Specifications and Guidelines v2.0, 2006.

[16] ENVI user manual 4.2, Research Systems Inc., 2003 http://www.gisits.com/otros/onlguide.pdf

[17] Vogelmann, J. E., D. Helder, R. Morfitt, M. J. Choate, J. M. Merchant, and H. Bulley, 2001, Effects of Landsat 5 Thematic Mapper and Landsat 7 Enhanced Thematic Mapper Plus radiometric and geometric calibrations and corrections on landscape characterization, *Remote Sensing of Environment*, 78:55-70.

[18] Huang, C., B. Wylie, C. Homer, L. Yang, and G. Zylstra, 2002. Derivation of a Tasselled cap transformation based on Landsat 7 at-sensor reflectance. *International Journal of Remote Sensing*, 23:1741-1748.

[19] Huang, C., L. Yang, C. Homer, B. Wylie, J. Vogelman, and T. DeFelice, 2001. At-satellite reflectance: a first order normalization of Landsat 7 ETM+ images: USGS Report http://landcover.usgs.gov/pdf/huang2.pdf

[20] Multi-resolution land characteristics 2001 (MRLC 2001) image processing procedure, EROS Data Center, United States Geological Survey Report, 9p. http://landcover.usgs.gov/pdf/image_preprocessing.pdf (online, accessed: April 2006)

[21] Irish, R. R., 2000, Landsat 7 science data user's handbook, National Aeronautics and Space Administration. http://ltpwww.gsfc.nasa.gov/IAS/handbook/handbook_toc.html (online, accessed: May 2006)

[22] Hall, F.G., D.E. Strebel, J.E. Nickeson and S.J. Goetz. 1991. Radiometric rectification: Toward a common radiometric response among multi-date, multi-sensor images. *Remote Sensing of Environment*, 35:11-27.

[23] Franklin, S., and M. Wulder, 2002. Remote sensing methods in medium spatial resolution satellite data land cover classification of large areas, Progress in Physical Geography, Vol. 26, No. 2, pp. 173-205.

[24] Mas, J.F., 1999. Monitoring land-cover changes: A comparison of change detection techniques. *International Journal of Remote Sensing*, 20: 139-152.

[25] Wulder, M. A., C.C. Dymond, J.C. White, D.G. Leckie and A.L. Carroll, 2006. Surveying mountain pine beetle damage of forests: A review of remote sensing opportunities. *Forest Ecology and Management*, 221: 27-41.

[26] Vogelmann, J.E., 1990. Comparison between two vegetation indices for measuring different types of forest damage in the north-eastern United States. *International Journal of Remote Sensing,* 11: 2281-2297.

[27] Falkenstrom, H. and Ekstrand, S., 2002. Evaluation of IRS-1c LISS-3 satellite data for defoliation assessment on Norway spruce and Scots pine. *Remote Sensing of Environment,* 82: 208-223.

List of Tables

Table 1. Landsat image characteristics.
Table 2. Example data values for each processing step based on a forest pixel arbitrarily selected from the time-2 TM image (with the results from the integrated protocol are in bold italic).
Table 3 Comparison of storage and computing time between standard and combined flow.

List of Figures

Figure 1. Merritt TSA study site located in southern British Columbia, Canada.
Figure 2. Flow chart describing the image processing steps.
Figure 3. Impact of scaling on wetness index density distribution (derived from time-1 dataset)

Tables

Table 1. Landsat image characteristics.

Input image	Sensor	Path	Row	Time of acquisition (GMT)	Date of acquisition
Date 1	ETM+	46	25	18:42:48	2002-08-14
	ETM+	46	26	18:43:12	2002-08-14
Date 2	TM	46	25	18:38:46	2004-09-28
	TM	46	26	18:39:10	2004-09-28

Table 2. Example data values for each processing step based on a forest pixel arbitrarily selected from the time-2 TM image (with the results from the integrated protocol are in bold italic).

Image channel	TM DN	ETM+ DN	Radiance ($W/(m^2\ sr\ \mu m)$).	Reflectance (%)		Normalized reflectance (%)	TCT wetness	
1	42	24	24	23	***24***	23	-18	***-20***
2	17	13	13	13	***13***	13		
3	12	12	12	11	***12***	11		
4	69	69	69	69	***69***	69		
5	35	35	35	35	***35***	35		
7	10	12	11	11	***12***	11		

Table 3. Comparison of storage and computing time between standard and combined flow. Computing platform is SUN4U workstation with 4GB RAM.

	Standard Flow			Combined Flow		
	Step	Storage (kB)	Time (sec.)	Step	Storage (kB)	Time (sec.)
	1	117,682	157	1	117,682	256
	2	117,682	191	2	39,228	164
	3	117,682	168			
	4	117,682	198			
	5	39,228	130			
Totals	5	509,956	844	2	156,910	420

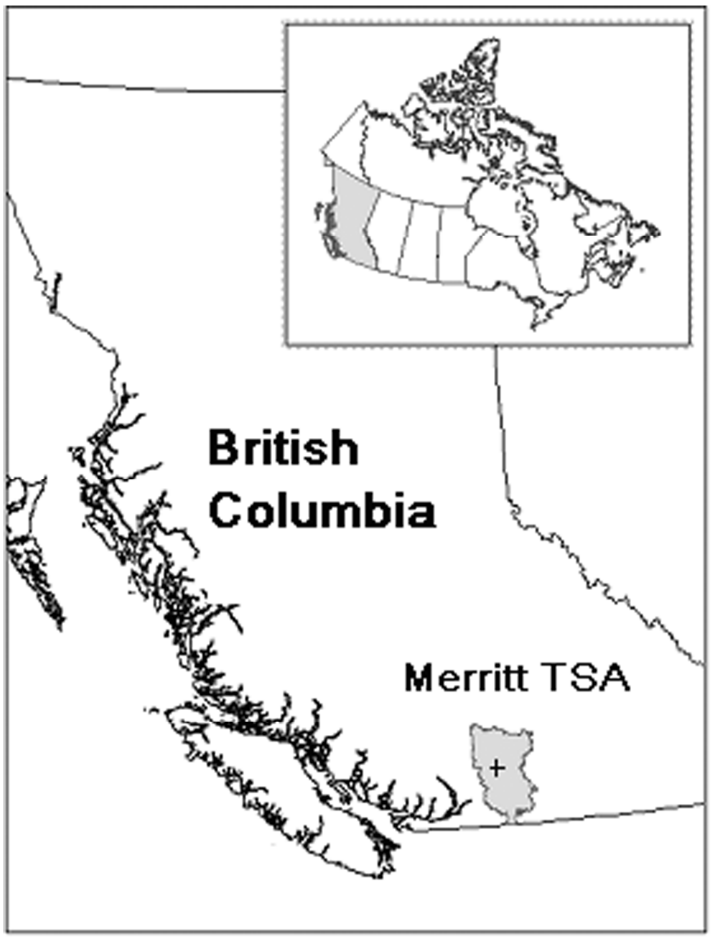

Figure 1

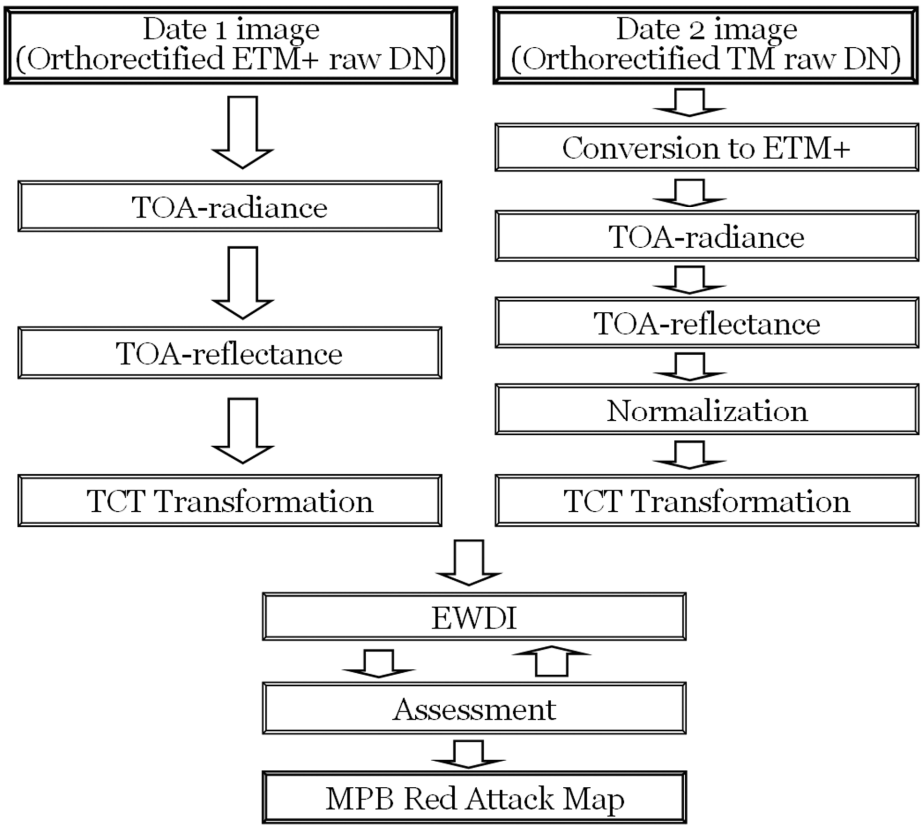
Date 1 image
(Orthorectified ETM+ raw DN)
Date 2 image
(Orthorectified TM raw DN)
Conversion to ETM+
TOA-radiance
TOA-radiance
TOA-reflectance
TOA-reflectance
Normalization
TCT Transformation
TCT Transformation
EWDI
Assessment
MPB Red Attack Map

Figure 2.

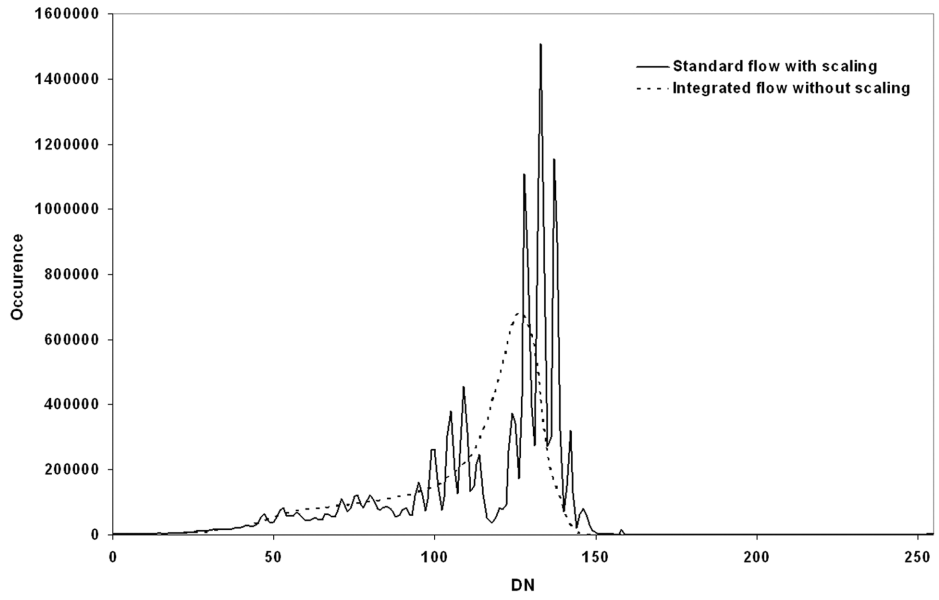
1600000
1400000
1200000
1000000
800000
600000
400000
200000
0
Occurence
0
50
100
150
200
250
DN
Standard flow with scaling
Integrated flow without scaling

Figure 3.